

# Thin-film magneto-inductive cables

R R A Syms<sup>1</sup>, L Solymar, I R Young and T Floume

Optical and Semiconductor Devices Group, EEE Department, Imperial College London,  
Exhibition Road, London SW7 2AZ, UK

E-mail: [r.syms@imperial.ac.uk](mailto:r.syms@imperial.ac.uk)

Received 25 October 2009, in final form 17 December 2009

Published 21 January 2010

Online at [stacks.iop.org/JPhysD/43/055102](http://stacks.iop.org/JPhysD/43/055102)

## Abstract

Magneto-inductive cables for low (ca 100 MHz) radio frequencies are demonstrated in thin-film form. 20 cm long resonant elements are formed using double-sided patterning of copper-clad polyimide, based on single-turn inductors and parallel-plate capacitors that use the substrate as an interlayer dielectric. Continuous cables are formed by overlaying elements, in an arrangement that allows a high, positive coupling coefficient ( $\kappa > 0.6$ ) to be achieved despite the use of a planar geometry. Equivalent circuit parameters are extracted from experiments on integrated coupling transducers, and propagation characteristics are compared with simple theory. Low propagation loss ( $4 \text{ dB m}^{-1}$  at 55 MHz, falling to  $2.3 \text{ dB m}^{-1}$  at 130 MHz) is demonstrated near the operating frequencies of magnetic resonance imaging, for a potential application as patient-safe cable in internal imaging.

## 1. Introduction

Recently there has been considerable interest in artificial electromagnetic structures that may have novel properties such as negative permittivity, permeability and refractive index [1–3]. Many are based on periodic arrays of resonant elements, and are therefore similar to those historically used in filters and slow wave circuits [4, 5]. However, wide-ranging research has extended the range of applications and operating frequencies very considerably [6–8].

One example of a simple metamaterial is the magneto-inductive (MI) waveguide [9], sometimes called a metasolenoid [10, 11]. The resonant element is a simple  $L$ – $C$  circuit, which is magnetically coupled to its neighbours by a mutual inductance  $M$  as shown in figure 1(a). There are two main variants: the axial (figure 1(b)) and planar (figure 1(c)) configurations, in which  $M$  is positive and negative, respectively. MI waves have been studied extensively, in one-dimensional (1D) waveguides [12–15] and in 2D and 3D arrays [16, 17]. Applications have been identified in magnetic field concentration [18], delay-lines [19], phase shifters [20], filters and splitters [21] and near-field lenses [22, 23].

A recent application is patient safety during *in vivo* internal magnetic resonance imaging (MRI) [24, 25], a generalization of earlier work in which co-axial cables carrying the signal from catheter-mounted detectors were subdivided using thin-film transformers [26]. Here, division into lengths shorter than

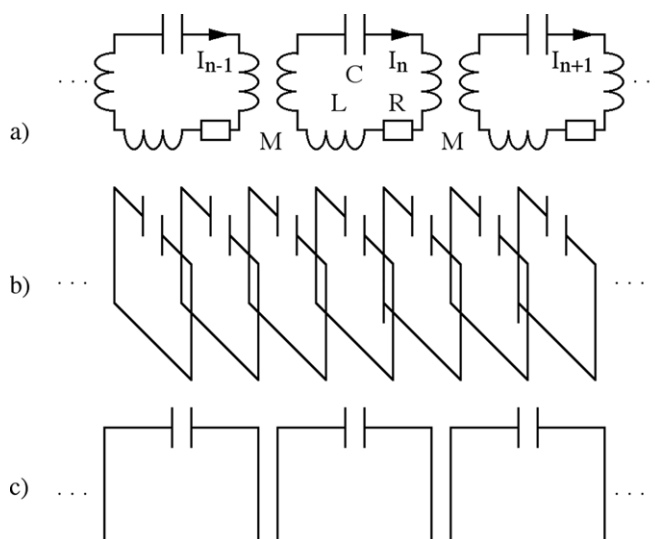


**Figure 1.** MI waveguide: (a) equivalent circuit, (b) and (c) axial and planar configurations.

the resonant length for external excitation prevents heating by the electric field of the powerful RF transmitter [27, 28]. The critical length is  $c/(2f\sqrt{\epsilon_r})$ , where  $c$  is the velocity of light,  $f$  is the frequency and  $\epsilon_r$  is the relative dielectric constant of any surrounding tissue. For  $^1\text{H}$  MRI in a 1.5 T field,  $f = 63.8 \text{ MHz}$ ,  $\epsilon_r = 77$  for human tissue and the critical length is around 27 cm.

<sup>1</sup> Author to whom any correspondence should be addressed.

Previously, MI waveguides have been constructed as discrete elements based on wire-wound [12] or printed circuit board [14] inductors and surface mount capacitors. However, construction has involved tedious assembly and tuning, and propagation losses have been extremely high. Taking into account the element spacing, published attenuation figures of  $\approx 1.5$  dB/element in [12] and  $\approx 0.12$  dB/element in [14] translate into propagation losses of  $\approx 150$  dB  $m^{-1}$  and  $\approx 50$  dB  $m^{-1}$ , respectively. These high values rule out most practical applications.

A key requirement is therefore low-cost fabrication of high-performance material, especially in long lengths, large areas or flexible formats. Metamaterials such as dipoles, Jerusalem crosses, wire pairs and split-ring resonators are now being fabricated using single-sided patterning of metal layers on flexible dielectric substrates [29–35]. This approach has been successful at terahertz frequencies, when only small effective component values are required and sufficient capacitance can be obtained using a coplanar geometry [32–35]. However, for a MI waveguide operating at megahertz frequencies, large values of  $L$  and  $C$  are required.

In this paper, a novel resonant element that allows low-loss, low frequency MI waveguides to be formed as continuous thin-film cables is introduced. Double-sided patterning of flexible copper-clad polyimide is used to form elements that combine loop inductors with integrated parallel-plate capacitors, and low-loss propagation is demonstrated at MRI frequencies over the 2 m lengths typical of catheter-based internal imaging probes. We believe these to represent the longest continuous metamaterial structures demonstrated to date. The approach also allows the incorporation of integrated coupling transducers. The design is introduced in section 2, fabrication and experimental characterization are described in section 3, experimental results are compared with the predictions of simple theory in section 4 and conclusions are presented in section 5.

## 2. Design

We first briefly review the underlying theory of MI waveguides [9]. Applying Kirchhoff's laws to the  $n$ th loop in figure 1(a), we obtain

$$\{j\omega L + 1/j\omega C + R\} I_n + j\omega M \{I_{n-1} + I_{n+1}\} = 0. \quad (1)$$

Here  $\omega = 2\pi f$  is the angular frequency and  $f$  is the corresponding temporal frequency. Here we have introduced resistors  $R$  to denote lossy inductors. Assuming that the currents  $I_n$  may be taken in the form of a travelling wave as  $I_n = I_0 \exp(-jnka)$ , where  $ka$  is the phase shift per element,  $k$  is the propagation constant and  $a$  is the period, the dispersion equation may be obtained as

$$\{1 - \omega_0^2/\omega^2 - j/Q\} + \kappa \cos(ka) = 0. \quad (2)$$

Here  $\omega_0 = 2\pi f_0 = 1/\sqrt{LC}$  is the angular resonant frequency,  $f_0$  is the corresponding temporal frequency,  $Q = \omega L/R$  is the  $Q$ -factor and  $\kappa = 2M/L$  is the coupling

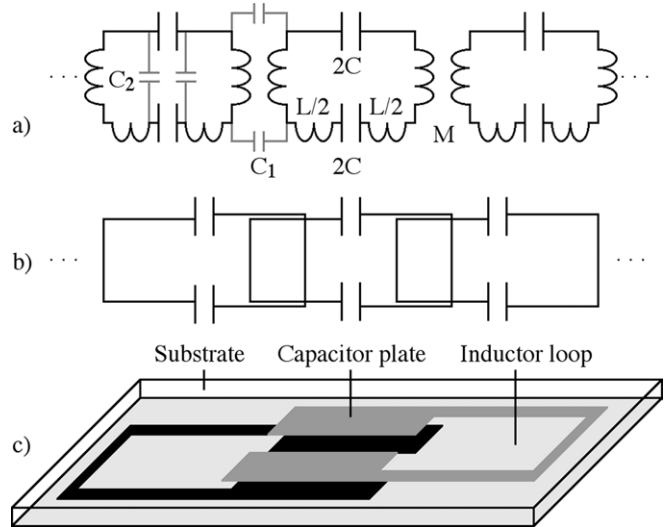


**Figure 2.** Thin-film MI cable: (a) equivalent circuit, (b) geometry, (c) resonant element.

coefficient. Assuming that  $k = k' - jk''$ , and losses are small, equation (2) may be approximated as

$$\begin{aligned} (1 - \omega_0^2/\omega^2) + \kappa \cos(k'a) &= 0, \\ k'a &= 1/\{\kappa Q \sin(k'a)\}. \end{aligned} \quad (3)$$

The first equation in (3) is the dispersion relation for loss-less waves. In the axial configuration,  $\kappa$  is positive, the waveguide supports forward waves and propagation is obtained only over the frequency band  $1/(1 + \kappa) \leq (\omega/\omega_0)^2 \leq 1/(1 - \kappa)$ , whose extent depends on the value of  $\kappa$ . The second equation shows that losses are lowest at mid-band ( $k'a \approx \pi/2$ ) and are reduced by a high  $Q$ -factor and a large coupling coefficient. In the planar configuration,  $\kappa$  is negative and backward waves are supported.

From the point of view of propagation loss, neither configuration is entirely satisfactory, since it is more often loss per metre that is important than loss per element. Planar elements can have a large physical extent in the direction of propagation, but have a relatively small coupling coefficient since  $|\kappa| < 1$  in this geometry. Experimental values are usually lower. Axial elements have a larger coupling coefficient, with a peak value that can approach  $\kappa = 2$ , but only if the period is so small that the distance propagated per element is extremely short.

We therefore introduce the modification shown in figure 2(a) (which omits resistive losses) in which the capacitor and inductor are each separated into two series-connected elements. This new arrangement has the same dispersion relation as that of figure 1(a). However, sub-division of the inductor allows adjacent resonators to be overlaid so that large, positive coupling is achieved in a planar geometry, as shown in figure 2(b). Sub-division of the capacitor allows the formation of high-value integrated parallel-plate components that use a thin substrate as a dielectric interlayer as shown in figure 2(c). Both sides of the substrate carry inductor loops and capacitor plates and a cable is realized by cascading sections so that inductors from adjacent elements overlay to form air-cored transformers.

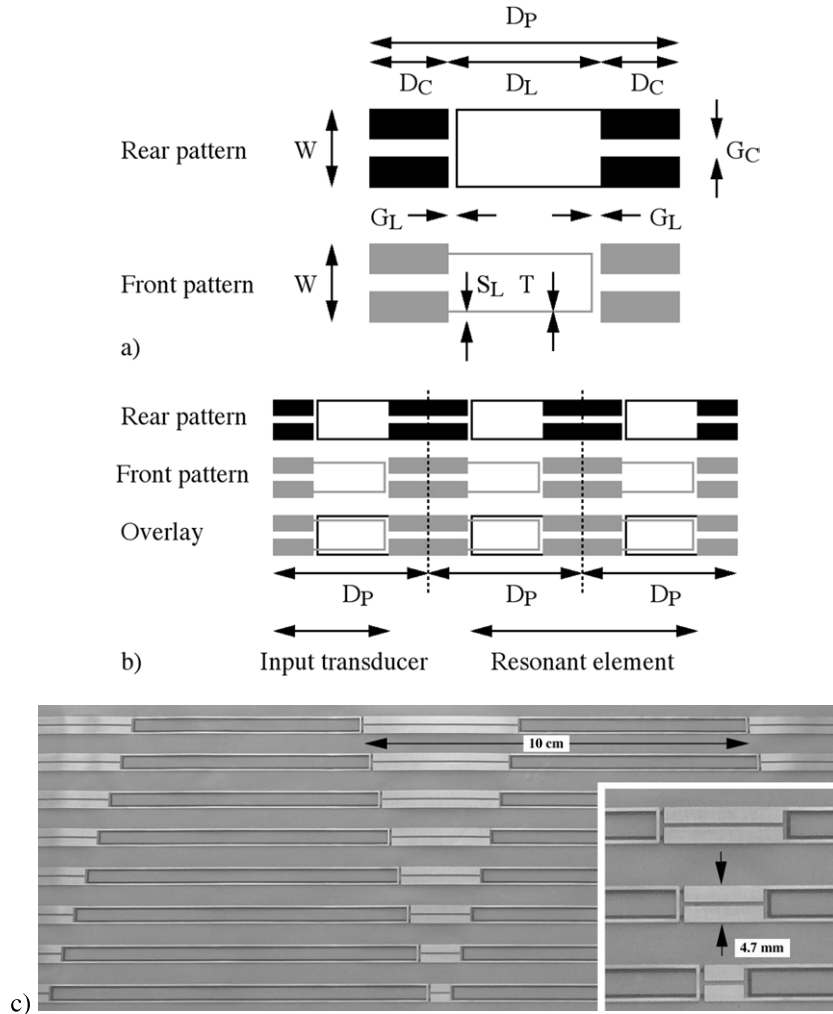


**Figure 3.** Thin-film MI cable: (a) layout parameters, (b) overall arrangement, (c) experimental realization in copper-clad polyimide.

In addition to reducing loss and improving manufacturability, this arrangement should reduce the relative size of non-nearest neighbour coupling, a feature that has complicated understanding and development of MI devices [15]. However, departures from ideal behaviour are still likely to arise from parasitic capacitances  $C_1$  between the tracks of overlapping inductors and  $C_2$  between the plates of adjacent capacitors. Careful choice of design dimensions is required to minimize their effect.

Cable layouts are specified using the parameters of figure 3(a), which shows one period. Elements are defined in terms of their overall width  $W$  and half-length  $D_P (= a)$ . Inductors are defined in terms of their half-length  $D_L$  and track width  $T$ . Capacitor plates are defined in terms of their half-length  $D_C = (D_P - D_L)/2$ , and a gap  $G_C$  between the plates is used to reduce  $C_1$ . A gap  $G_L$  is used to separate the inductors and capacitors, and a further transverse separation  $S_L$  is introduced between the tracks on either side of the substrate to reduce  $C_2$ . Periodic repetition allows a complete cable to be defined, together with inductors that can act as integrated transducers for input and output coupling as shown in figure 3(b). The overall length of a cable with  $N$  resonant elements is then  $(N + 1)D_P$ .

### 3. Fabrication and experimental characterization

Prototype thin-film MI cables were fabricated in 2 m lengths by the UK company Clarydon (Willenhall, West Midlands), using double-sided patterning of copper-clad polyimide. The starting material was  $25 \mu\text{m}$  thick Kapton® HN (DuPont, Circleville, OH), coated on each side with a  $35 \mu\text{m}$  thick pressure-bonded layer of copper. The copper was patterned by lithography and wet chemical etching, using two consecutive exposures to a pair of 1 m-long photomasks whose layouts were defined by a Gerber file. Registration to the Kapton sheet was achieved using mechanical alignment pins.

Dimensions for operation at MRI frequencies were estimated from an earlier work. PCBs were fabricated as panels measuring  $300 \text{ mm} \times 2 \text{ m}$ . Each panel contained three repeats of an array containing eight different MI cables with the parameters given in table 1. In each case, the same value of  $D_P = 10 \text{ cm}$  was used, so that the overall element length of  $20 \text{ cm}$  was less than the critical value given earlier. A 2 m long panel then contained  $200/10 - 1 = 19$  resonant elements. The overall width  $W$  was taken as  $4.7 \text{ mm}$  throughout, to place the conductors on the diameter of an 8Fr ( $2.7 \text{ mm}$  diameter) catheter. The lengths  $D_L$  and  $D_C$  of the inductors

**Table 1.** Layout and equivalent circuit parameters of experimental thin-film MI cables.

Design	$D_L$ (mm)	$D_C$ (mm)	$L$ (nH)	$C$ (pF)	$f_0$ (MHz)	$f'_0$ (MHz)	$Q$	$\kappa$
A	60.0	20.0	178.4	36.4	62.5	55.5	36.0	0.615
B	65.0	17.5	186.1	30.3	67.0	57.5	36.5	0.625
C	70.0	15.0	196.2	26.3	70.3	61.0	38.0	0.635
D	75.0	12.5	206.8	21.2	76.0	65.0	39.5	0.645
E	80.0	10.0	217.8	17.4	81.8	70.5	41.5	0.655
F	85.0	7.5	229.7	13.0	92.0	79.5	44.0	0.665
G	90.0	5.0	240.9	9.6	104.5	95.0	48.0	0.675
H	95.0	2.5	249.5	6.0	130.0	130.0	55.0	0.690

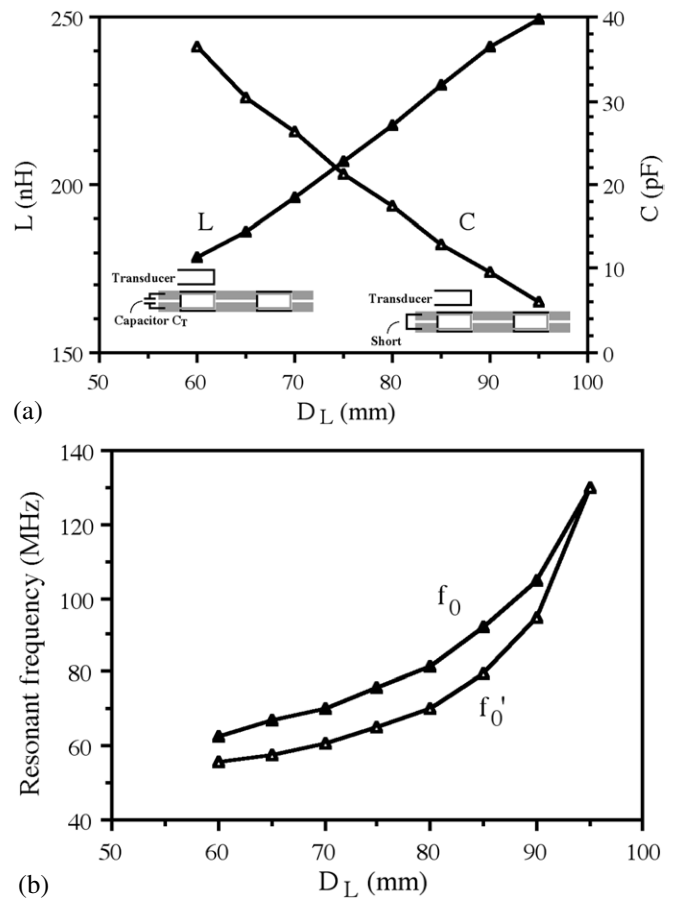
and capacitors were varied across the array to obtain a variation in the resonant frequency  $f_0$ . The widths of all narrow features including track widths and clearance gaps ( $T$ ,  $G_C$ ,  $G_L$  and  $S_L$ ) were taken as 0.5 mm, the minimum feature size that could be patterned reliably over a 2 m length. Figure 3(c) shows a completed array with design A at the top and H at the bottom, from which individual guides can be separated using a scalpel.

Electrical performance was measured using an Agilent E5061A Electronic Network Analyser. The equivalent circuit parameters are given in table 1 and were extracted from measurements of integrated transducers. A large capacitor  $C_T = 1$  nF was first soldered across a transducer, which effectively comprised half an element, to create a new element defined mainly by  $L/2$  and  $C_T$ . The resonant frequency  $f_{T1}$  of this element was found by inductive probing, and used to estimate  $L$ . The capacitor was then removed, and a short circuit soldered across the two half-length capacitor plates at the substrate rear below the transducer connections, to create a further new resonant element now defined mainly by  $L/2$  and  $C/2$ . The resonant frequency  $f_{T2} = f_0/2$  of this element was then used to estimate  $C$ . Component values extracted from either end of the same cable were consistent, suggesting good dimensional control. Figure 4(a) shows the variation of  $L$  and  $C$  with  $D_L$ ; both vary linearly to good approximation. Figure 4(b) shows the corresponding variation of  $f_0$ , which shows that the designs straddle the frequency range from 63.8 MHz to 127.6 MHz, corresponding to  $^1\text{H}$  MRI at fields between 1.5 T and 3 T.

The extracted capacitance may be compared with an estimate  $C_{\text{est}} = D_C(W - G_C)\epsilon_0\epsilon_r/2t$  obtained from a parallel plate model, where  $\epsilon_0 = 8.85 \times 10^{-12}$  F m $^{-1}$ , and  $\epsilon_r = 3.5$  is now the relative dielectric constant and  $t = 25$   $\mu\text{m}$  is the thickness of the polyimide sheet. The extracted values are generally smaller than these estimates, suggesting experimental error in the determination of  $f_{T2}$  (and hence also in  $f_0$ ) caused by proximity to the propagating band.

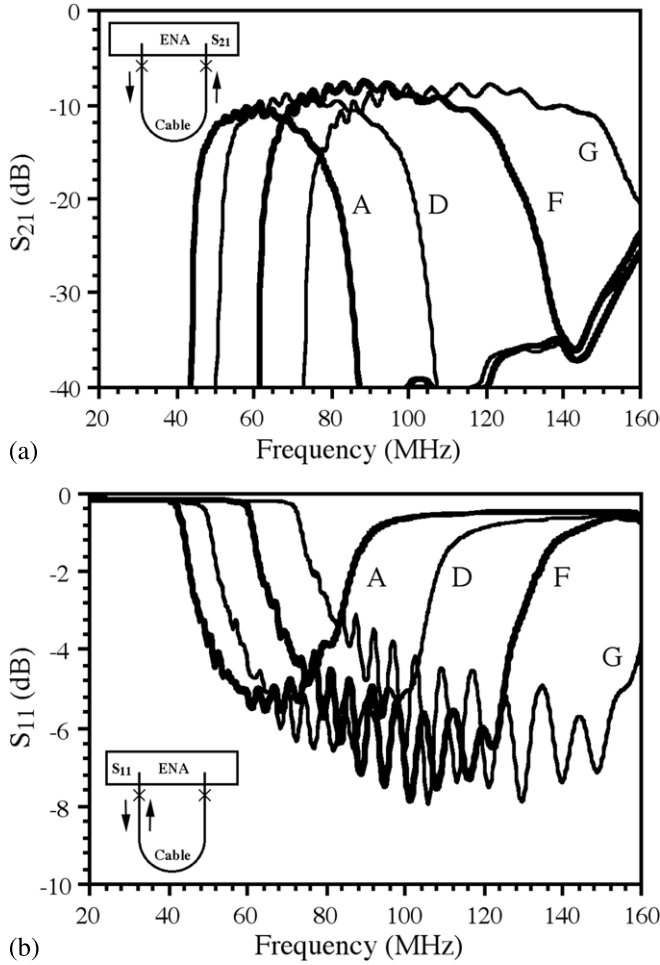
Cable properties were determined after attaching SMA connectors to the input and output transducers and connecting to the network analyser. The cables could be flexed gently without significant variations in transmission. However, folding the cables so resonators at different points could couple magnetically did introduce changes. Figure 5 shows the frequency variation of the  $S$ -parameters of 2 m lengths of four different cables (A, D, F and G). The remaining designs have equivalent performance at appropriate frequencies.

Figure 5(a) shows the frequency variation of  $S_{21}$ . In each case, propagation is band-limited, with the centre frequency



**Figure 4.** Experimental variation with the inductor loop length  $D_L$  of (a) the inductance  $L$  and the capacitance  $C$ , and (b) the resonant frequencies  $f_0$  and  $f'_0$ .

and bandwidth increasing from design A to G. Out of band, there is increasing transmission at higher frequencies, which is attributed to the parasitic capacitance  $C_1$  in the transformers. Overall transmission also increases from design to design, but relatively slowly. For design A, for example, propagation is obtained from 44 to 88 MHz, and minimum insertion loss of around 11 dB is obtained near 63.8 MHz frequency. For design G, minimum loss has reduced to around 7.5 dB, and this design would be suitable for operation at 127.6 MHz. Figure 5(b) shows the frequency variation of  $S_{11}$ . In each case, impedance matching is moderate, with a minimum return of around  $-5$  dB for design A reducing to  $-7$  dB for design G. These results suggest that the majority of the insertion loss must be due to attenuation rather than coupling loss.



**Figure 5.** Frequency variation of (a)  $S_{21}$  and (b)  $S_{11}$  for 2 m lengths of four different thin-film MI cables.

After measurement, lines were attached to the outside of 8 Fr catheters using heat-shrink tubing, and re-measured. The only change in performance was a slight increase in centre frequency following from the reduction in inductance  $L$  caused by the change in geometry.

#### 4. Comparison with theory

To compare the experimental results with theory, a method of estimating  $S$ -parameters is required. We use a simple approach that ignores multiple reflections, but which also neglects loss in calculation of reflection coefficients and hence is valid only for intermediate attenuation. To estimate reflection losses, we assume the geometry of figure 6(a), where a semi-infinite line ending at element 0 is terminated using a resistor  $R_L$  via an inductive transducer. Other resistive losses are ignored. For the final elements, Kirchhoff's laws give

$$\begin{aligned} \{j\omega L + 1/j\omega C\} I_0 + j\omega M \{I_{-1} + I_L\} &= 0, \\ \{R_L + j\omega L/2\} I_L + j\omega M I_0 &= 0. \end{aligned} \quad (4)$$

From the second equation in (4) the load current can be found. Substituting into the first equation, we obtain

$$\{j\omega L + 1/j\omega C + Z_L\} I_0 + j\omega M I_{-1} = 0. \quad (5)$$

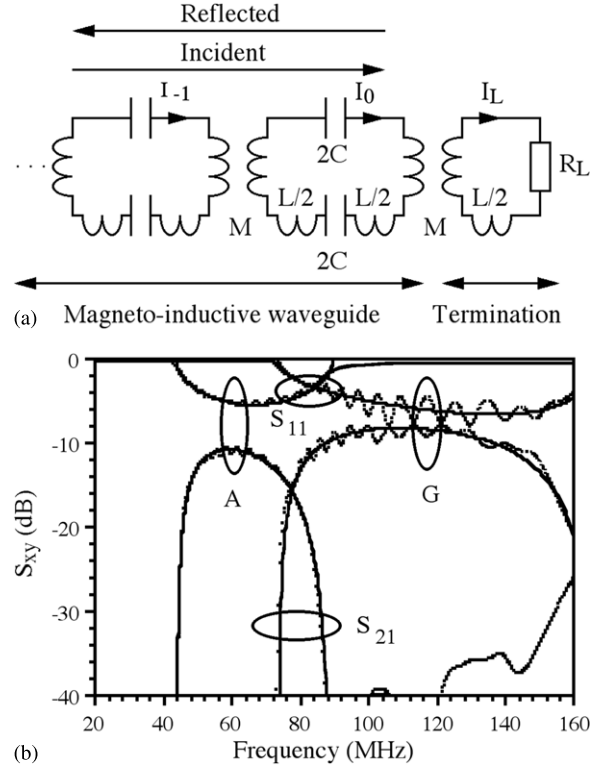


**Figure 6.** (a) Equivalent circuit of a terminated MI waveguide; (b) comparison between  $S$ -parameter measurements and theory for two different thin-film MI waveguides. Points are experimental data, and lines are theory.

Here  $Z_L = \omega^2 M^2 / \{R_L + j\omega L/2\}$  is an effective load impedance. A solution is now attempted as a sum of counter-propagating waves, i.e. as  $I_n = I_I \exp(-jnka) + I_R \exp(+jnka)$  where  $I_I$  and  $I_R$  are the incident and reflected wave amplitudes. This solution automatically satisfies the loss-less recurrence equations away from the termination. Substituting into equation (5), and using these relations, we can obtain the reflection coefficient  $\Gamma = I_R/I_I$  for current waves as

$$\Gamma = -\{Z_L - Z_0\} / \{Z_L + Z_0^*\} \quad (6)$$

Here  $Z_0$  is the characteristic impedance of a MI waveguide, previously found in [8] as

$$Z_0 = j\omega M \exp(-jka) \quad (7)$$

and  $Z_0^*$  is the complex conjugate of  $Z_0$ . At mid-band ( $ka = \pi/2$ ),  $Z_0$  is real and has the value  $Z_{0M} = \omega_0 M$ . In principle, it should be possible to match  $Z_{0M}$  to a real resistive load by appropriate choice of  $M$  and by making the effective termination  $Z_L$  real at  $f_0$ , using an additional series capacitor. In this case we simply require  $\omega_0 M = R_L$ .

Including propagation losses arising from the imaginary part of the propagation constant, but neglecting multiple reflections, the scattering parameters of an  $N$ -element waveguide with identical terminations at either end may then be expressed in dB as

$$S_{11} \approx 10 \log_{10} \{|\Gamma|^2\}, \quad (8)$$

$$S_{21} \approx 10 \log_{10} \{(1 - |\Gamma|^2) \exp(-2Nk''a) (1 - |\Gamma|^2)\}.$$



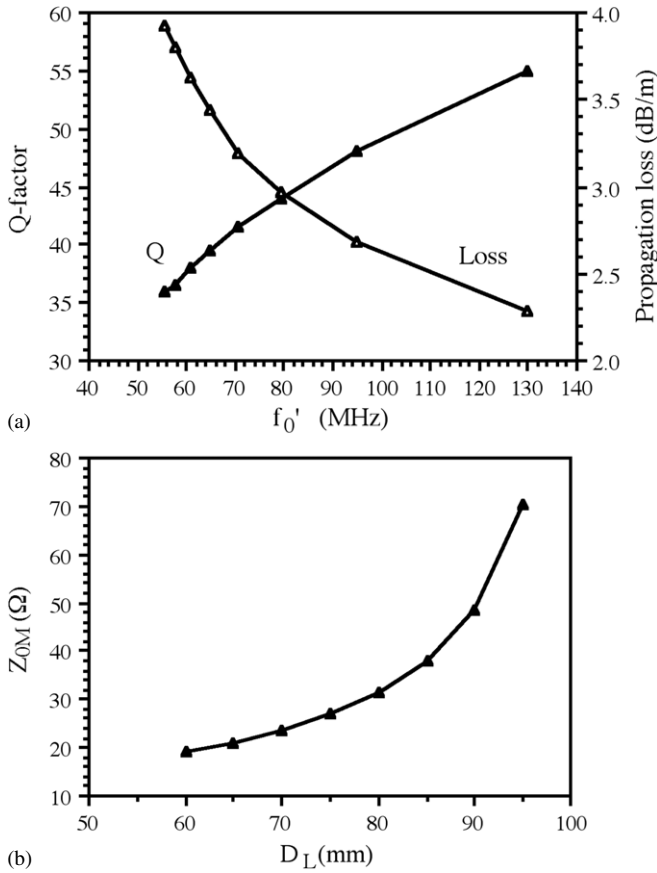


**Figure 7.** (a) Variation with resonant frequency  $f'_0$  of the  $Q$ -factor and the propagation loss; (b) variation with the inductor loop length  $D_L$  of the mid-band impedance  $Z_{0M}$ .

Theoretical estimates obtained from equations (3) and (6)–(8) were compared with experimental data as follows. The inductance  $L$  was assumed to be accurately determined. The resonant frequency  $f'_0$  (an approximation to  $f_0$  obtained by matching theory to experiment),  $Q$ -factor and coupling coefficient  $\kappa$  were then adjusted to fit the centre frequency, bandwidth and maximum transmission, respectively. Figure 6(b) shows a typical comparison between experiment and theory for the frequency variation of  $S$ -parameters of designs A and G, assuming  $R_L = 50 \Omega$ . Generally, the agreement is excellent, although the theory clearly cannot predict the oscillations arising from multiple reflections.

The fitting parameters are detailed in table 1, and the variation of  $f'_0$  with  $D_L$  is superimposed on figure 4(b) for comparison with the earlier estimate. Discrepancies between  $f'_0$  and  $f_0$  confirm the small inaccuracy in experimental determination of the latter. The  $Q$ -factor is modest, rising quasi-linearly with  $f'_0$  from 36 in design A to 55 in design H, as shown in figure 7(a). The coupling coefficient  $\kappa$  rises slowly with  $D_L$  from 0.61 to 0.69, suggesting that the central sections of the inductors provide slightly more effective coupling than the ends. The combination of rising  $Q$ -factor and coupling coefficient causes a reduction in propagation loss. At mid-band, the loss per element can be found in dB from

equation (3) as

$$\text{Loss/element} = 10 \log_{10} \{ \exp(-2/\kappa Q) \}. \quad (9)$$

This value can be converted into an equivalent loss per metre by dividing by the repeat distance  $D_P (= a)$ . Figure 7(a) also shows the variation of propagation loss with  $f'_0$ . The loss falls from  $\approx 0.4$  to  $\approx 0.23$  dB/element (or 4 to 2.3 dB  $m^{-1}$ ) over the range shown. Compared with earlier MI waveguides [14], the second figure represents a 20-fold reduction in loss per metre, largely due to the increased size of the new elements.

Finally, we show in figure 7(b) the variation with the inductor length  $D_L$  of the mid-band impedance  $Z_{0M}$ . The impedance rises from  $\approx 20 \Omega$  in design A to  $\approx 70 \Omega$  in H, due to a combination of a slow increase in  $M$  and a more rapid rise in  $f_0$ . Since the values are close to  $50 \Omega$ , it should be relatively simple to reduce coupling losses by small changes in layout.

## 5. Conclusions

Low-loss propagation of MI waves has been demonstrated using thin-film cables fabricated entirely by double-sided patterning of copper-clad polyimide. The resonant elements are formed using single-turn inductors and parallel-plate capacitors that use the substrate as a dielectric interlayer. Integrated coupling transducers are also formed from single-turn inductors. Large, positive coupling between elements is obtained despite the use of a planar arrangement, and the availability of high-value integrated capacitors allows operation at low (100 MHz) frequencies. The fabrication method is intrinsically low-cost and extensible to long lengths using step-and-repeat patterning, and should allow rapid development of other thin-film MI components such as splitters and filters. Low insertion and propagation losses have been demonstrated over 2 m lengths. Experimental measurements of  $S$ -parameter variations have been compared with the predictions of a simple theoretical model, and good agreement has been obtained. Further improvements in performance and a reduction in element size should follow from the use of multi-turn inductors. These aspects are now being investigated.

Finally we note that a time-varying external magnetic field can induce voltages in the open loops. However, if the external field is slowly varying in space, the overall voltage can be minimized by replacing open loops with figure-of-eight windings, so that induced voltages in each half-winding at least partly cancel. This arrangement would avoid RF heating or damage by the transmit field in a MRI scanner, together with any substantial modification to the excitation pattern [36]. Voltages induced by faster-varying fields from local dipole distributions would not necessarily be subject to such cancellation. However, any resulting signals would be encoded in frequency space by the gradient fields, and could be separated out by scanner software. Such signals can be used for visualizing the track of the cable [37].

## References

- [1] Veselago V G 1968 The electrodynamics of substances with simultaneously negative values of  $\epsilon$  and  $\mu$  *Sov. Phys.—Usp.* **10** 509–14

- [2] Pendry J B, Holden A J, Robbins D J and Stewart W J 1999 Magnetism from conductors and enhanced nonlinear phenomena *IEEE Trans. Microw. Theor. Tech.* **MTT 47** 2075–84
- [3] Smith D R, Padilla W J, Vier D C, Nemat-Nasser S C and Schultz S 2000 Composite medium with simultaneously negative permeability and permittivity *Phys. Rev. Lett.* **84** 4184–7
- [4] Brillouin L 1953 *Wave Propagation in Periodic Structures: Electric Filters and Crystal Lattices* 2nd edn (New York: Dover)
- [5] Silin R A and Sazonov V P 1971 *Slow Wave Structures* (Boston SPA, UK: National Lending Library for Science and Technology)
- [6] Caloz C and Itoh T 2006 *Electromagnetic Metamaterials: Transmission Line Theory and Microwave Applications* (Hoboken, NJ: Wiley Interscience)
- [7] Engheta N and Ziolkowski R W 2006 *Metamaterials* (New York: Wiley)
- [8] Solymar L and Shamonina E 2009 *Waves in Metamaterials* (Oxford: Oxford University Press)
- [9] Shamonina E, Kalinin V A, Ringhofer K H and Solymar L 2002 Magneto-inductive waveguide *Electron. Lett.* **38** 371–3
- [10] Maslovski S, Ikonen P, Kolmakov I and Tretyakov S 2005 Artificial magnetic materials based on the new magnetic particle: metasolenoid *Prog. Electromagn. Res.* **54** 61–81
- [11] Jylhä L, Maslovski S and Tretyakov 2009 Traveling waves along the metasolenoid *Progress in Electromagnetics Research Symp. (Cambridge, MA, 26–29 March 2009)*
- [12] Wiltshire M C K, Shamonina E, Young I R and Solymar L 2003 Dispersion characteristics of magneto-inductive waves: comparison between theory and experiment *Electron. Lett.* **39** 215–17
- [13] Shamonina E and Solymar L 2004 Magneto-inductive waves supported by metamaterial elements: components for a one-dimensional waveguide *J. Phys. D: Appl. Phys.* **37** 362–7
- [14] Syms R R A, Young I R and Solymar L 2006 Low-loss magneto-inductive waveguides *J. Phys. D: Appl. Phys.* **39** 3945–51
- [15] Syms R R A, Sydoruk O, Shamonina E and Solymar L 2007 Higher order interactions in magneto-inductive waveguides *Metamaterials* **1** 44–51
- [16] Shamonina E, Kalinin V A, Ringhofer K H and Solymar L 2002 Magnetoinductive waves in one, two and three dimensions *J. Appl. Phys.* **92** 6252–61
- [17] Syms R R A, Shamonina E and Solymar L 2005 Positive and negative refraction of magnetoinductive waves in two dimensions *Eur. Phys. J. B* **46** 301–8
- [18] Wiltshire M C K, Shamonina E, Young I R and Solymar L 2003 Resonant magnetic concentrator *Progress in Electromagnetics Research Symp. (Honolulu, HI, USA 13–16 October 2003)*
- [19] Freire M J, Marques R, Medina F, Laso M A G and Martin F 2004 Planar magneto-inductive wave transducers: theory and applications *Appl. Phys. Lett.* **85** 4439–41
- [20] Nefedov I S and Tretyakov S A 2005 On potential applications of metamaterials for the design of broadband phase shifters *Microw. Opt. Tech. Lett.* **145** 98–102
- [21] Syms R R A, Shamonina E and Solymar L 2006 Magneto-inductive waveguide devices *IEE Proc. Microw. Antennas Propag.* **153** 111–21
- [22] Freire M J and Marques R 2005 Planar magnetoinductive lens for three-dimensional subwavelength imaging *Appl. Phys. Lett.* **86** 182505
- [23] Sydoruk O, Shamonin M, Radkovskaya A, Zhuromskyy O, Shamonina E, Trautner R, Stevens C J, Faulkner G, Edwards D J and Solymar L 2007 Mechanism of subwavelength imaging with bilayered magnetic metamaterials: theory and experiment *J. Appl. Phys.* **101** 073903
- [24] Syms R R A, Solymar L and Young M R 2009 MR-safe cables—an application of magneto-inductive waves? *Proc. 3rd Int. Cong. on Advanced Electromagnetic Materials in Microwaves and Optics (London, UK, 30 August–4 September)* pp 221–3
- [25] Syms R R A, Solymar L and Young I R Periodic analysis of MR-safe transmission lines *IEEE J. Sel. Top. Quantum Electron.* at press doi:10.1109/JSTQE.2009.2032782
- [26] Weiss S, Vernickel P, Schaeffter T, Schulz V and Gleich B 2005 Transmission line for improved RF safety of interventional devices *Magn. Reson. Med.* **54** 182–9
- [27] Konings M K, Bartels L W, Smits H F M and Bakker C J G 2000 Heating around intravascular guidewires by resonating RF waves *J. Magn. Reson. Imag.* **12** 79–95
- [28] Nitz W R, Oppelt A, Renz W, Manke C, Lenhart M and Link J 2001 On the heating of linear conductive structures as guidewires and catheters in interventional MRI *J. Magn. Reson. Imag.* **13** 105–14
- [29] Shelton D, Tharp J, Zummo G, Folks W and Boreman G 2007 Fabrication of periodic microstructures on flexible polyimide membranes *J. Vac. Sci. Technol. B* **25** 1827–31
- [30] Shelton D W, Cleary J W, Ginn J C, Wadsworth S L, Peale R E, Kotter D K and Boreman G D 2008 Gangbuster frequency-selective surface metamaterials in terahertz band *Electron. Lett.* **44** 1288
- [31] Awad M, Nagel M and Kurz H 2008 Negative-index metamaterial with polymer-embedded wire-pair structures at terahertz frequencies *Opt. Lett.* **33** 2683–5
- [32] Tao H, Strikwerda A C, Fan C, Bingham C M, Padilla W J, Zhang X and Averitt R D 2008 Terahertz metamaterials on free-standing highly-flexible polyimide substrates *J. Phys. D: Appl. Phys.* **41** 232004
- [33] Tao H, Strikwerda A C, Fan K, Bingham C, Landy N I, Shrekhamer D, Pilon D, Padilla W J, Zhang X and Averitt R D 2009 Flexible and reconfigurable THz metamaterials *SPIE Proc.* **7394** 73940D
- [34] Peralta X G *et al* 2009 Large-area metamaterials on thin membranes for multilayer and curved applications at terahertz and higher frequencies *Appl. Phys. Lett.* **94** 161113
- [35] Miyamaru F, Takeda M W and Yaima K 2009 Characterization of terahertz metamaterials fabricated on flexible plastic films: towards fabrication of bulk metamaterials in terahertz region *Appl. Phys. Exp.* **2** 042001
- [36] Krafft A, Müller S, Umatham R, Semmler W and Bock M 2006 B<sub>1</sub> field-insensitive transformers for RF-safe transmission lines *Magn. Res. Mater. Phys.* **19** 257–66
- [37] Burl M, Coutts G A, Herlihy D, Hill-Cottingham R, Eastham J E, Hajnal J V and Young I R 1999 Twisted-pair RF coil suitable for locating the track of a catheter *Magn. Reson. Med.* **41** 636–8